16. Nageswar, R. C. *et al.*, Synthesis and antithrombotic activity study of some new thienopyridine derivatives. *Lett. Org. Chem.*, 2011, **8**(6), 412–415.
17. Nageswar, R. C., Mamidisetty, B., Mahesh, R. G. and Padi, P. R., Synthesis and pharmacological evaluation of 5-[2′-(1H-tetrazol-5-yl)-biphenyl-4-ylmethyl]-4,5,6,7-tetrahydro-thieno[3,2-c]pyridine derivatives as platelet aggregation inhibitors. *J. Saudi Chem. Soc*., 2011, DOI: 10.1016/j.jscs.2011.10.016.
18. Lacefield, *et al*., Arylacetylene compounds as antithrombotic agents. Eli Lilly and Company, Patent number US 3968251, July 1976.
19. Kotian, P. L. *et al*., Design, parallel synthesis, and crystal structures of biphenyl antithrombotics as selective inhibitors of tissue factor FVIIa complex. Part 1: Exploration of S2 pocket pharmacophores. *Bioorg. Med. Chem*., 2009, **17**, 3934–3958.
20. Mahipal, T. O. P., Karthikeyan, C., Moorthy, N. S. and Trivedi, P., 3D QSAR of aminophenyl benzamide derivatives as histone deacetylase inhibitors. *Med. Chem*., 2010, **6**, 277–285.
21. Dixon, S. L., Smondyrev, A. M. and Rao, S., PHASE: A novel approach to pharmacophore modeling and 3D database searching. *Chem. Biol. Drug Des.*, 2006, **67**, 370–372.
22. Dixon, S. L., Smondyrev, A. M., Knoll, E. H., Rao, S. N., Shaw, D. E. and Friesner, R. A., PHASE: a new engine for pharmacophore perception, 3D QSAR model development, and 3D database screening: 1. Methodology and preliminary results. *J. Comput. Aided Mol. Des.*, 2006, **20**, 647–671.
23. Kolossvary, I. and Guida, W. C., Low mode search: an efficient, automated computational method for conformational analysis application to cyclic and acyclic alkanes and cyclic peptides. *J. Am. Chem. Soc*., 1996, **118**, 5011–5019.
24. Shelke, S. M., Bhosale, S. H., Dash, R. C., Suryawanshi, M. R. and Mahadik, K. R., Exploration of new scaffolds as potential MAO-A inhibitors using pharmacophore and 3D-QSAR based *in silico* screening. *Bioorg. Med. Chem. Lett.*, 2011, **21**, 2419–2424.
25. Golbraikh, A., Shen, M., Xiao, Z., Xiao, Y. D., Lee, K. H. and Tropsha, A., Rational selection of training and test sets for the development of validated QSAR models. *J. Comput. Aided Mol. Des*., 2003, **17**, 241–253.
26. Friesner, R. A. *et al.*, Glide: a new approach for rapid, accurate docking and scoring. 1. Method and assessment of docking accuracy. *J. Med. Chem.*, 2004, **47**, 1739–1749.
27. Friesner, R. A. *et al.*, Extra precision glide: docking and scoring incorporating a model of hydrophobic enclosure for protein–ligand complexes. *J. Med. Chem.*, 2006, **49**, 6177–6196.
28. Schrödinger Suite 2009 Protein Preparation Wizard; Epik version 2.0; Impact version 5.5. Schrödinger, LLC, New York.

ACKNOWLEDGEMENTS. A.N.J. thanks the Council of Scientific and Industrial Research – Unit for Research and Development of Information Products, Pune for providing financial support. We also thank the Centre for Development of Advanced Computing, Bioinformatics Resource and Application Facility, Pune, for providing computational facility.

Received 28 February 2013; revised accepted 3 September 2013

# Detection and size distribution analysis of ice floes near Antarctica using RISAT-1 imagery

**S. Srisudha, A. Senthil Kumar*, D. S. Jain and V. K. Dadhwal**

National Remote Sensing Center (ISRO), Balanagar, Hyderabad 500 625, India

**This study shows that C-band FRS-1 image mode data from RISAT-1 mission can be exploited to identify and monitor ice floes in the polar regions. The ice floes size distribution plays a vital role in understanding both ice motion dynamics and polar species habitat in the sea-ice zones. An automated algorithm was chosen here as against manual approach for identification of the floes for operational ice-floe mapping. The assessment of mapping accuracy was estimated to be about 80%. This exercise may help initiate temporal variations of the ice-floe size distribution to support ice-floe formation processes and climatic impact studies.**

**Keywords:** Ice-floe detection, polar sea-ice, radar imagery, size distribution analysis.

ICE floes result from fracturing of thick sea-ice in the polar regions largely due to strong winds and waves that prevail in these regions seasonally. These ice floes have different shapes and sizes ranging from about a metre to a few kilometres. The size distribution of these floes has become an important model parameter in the dynamic and thermodynamic processes of sea-ice area. The melting rate of ice floes, for example, depends on the ice-floe size; smaller the ice floes higher is the lateral melting[1]. Also, it was shown that momentum transferred from the atmosphere to ice would vary with the ice-floe size[2]. The size distribution and shape of ice floes would provide a clue to the understanding of ice-floe formation processes[3,4]. Besides, such analyses provide a lead to ice motion tracking as a part of warning alerts of ship routing. Also, polar species like walrus are attracted to ice floes that can support their weight; the ice-floe size distribution is necessary to determine the links between species habitat and sea-ice[5].

Though many research studies based on sea truth survey expeditions have been carried out routinely for ice-floe monitoring, space-borne remotely sensed data analysis stands undisputed as the only means of operationally monitoring ice-floe motion analysis by virtue of its unique advantages of larger coverage and high repeat cycle capabilities of the present-day on-board sensors. The sensors operating in the microwave region of the electromagnetic spectrum are better suited than their

*For correspondence. (e-mail: senthilkumar_a@nrsc.gov.in)

optical counterparts, since most parts of the polar regions are under persistent cloud cover throughout the year.

Isolating the ice floes in the remotely sensed data is a challenging task – both manual and by machine. The ice floes float in the background sea-ice in different shapes and sizes. These are not fully separated from one another, and do not have clear demarcation to decide their boundaries. In addition, grey-level difference between the background and the ice floes is not significantly high, especially for medium-sized floes (typically 50–500 pixels), and also varies across the image to fix a global threshold value as is done in many image segmentation applications.

Keeping in mind an operational approach for periodic monitoring of ice-floe movement, we adapted a fully automated algorithm[1] proposed earlier with ERS-1 imagery for ice floes. This method first works on local but dynamically varying image segmentation thresholding based on estimated bi-Gaussian distribution function of grey levels, followed by restricted region growing strategy to retain size and shape of the isolated floe areas. A full description of the algorithm is beyond the scope of this communication. The reader is referred to detailed description of the procedure in the literature[1].

Input datasets for this analysis were collections of RISAT-1 SAR over the Antarctica regions acquired on 3 December 2012 (orbit: 3743) in FRS-1 image mode with 9 m resolution. RISAT-1 is the first Indian space borne mission with active imaging sensor on-board operating in C-band, built with capabilities of imaging in four different modes in its both ascending and descending passes. Details of the RISAT-1 sensor mode descriptions[6], data processing[7] and users' data products[8] are available in the literature. For the present study, we have employed four scenes of FRA-1 data processed to level-1 (ground range) correction from operational data processing systems. These scenes were further mosaicked to get a seamless image continuity before extracting regions of interest. Figure 1 shows the mosaicked image strip with scene layout shown on the top left. Also shown are the regions (1 to 4) selected for floe size distribution analysis. Details of the image size for each selected region along with its centre positional map locations are given in Table 1.

Four regions of interest shown in Figure 1 are subjected to automated ice-floe size distribution algorithm. Since the ice floes are irregular in shape and also a large variation in size is observed, these were classified into the following bin sizes similar to the levels proposed for Arctic ice-floe studies[1]. To further quantify the size distribution, median of the range pixels is considered for estimating equivalent diameter values (Table 2).

The selected regions are processed using the algorithm mentioned above. Results obtained for region-3 are shown as an example in Figure 2. Figure 2 *a* shows the original image which when processed yields segmented ice-floe regions of different sizes. This image is then subjected to probabilistic labelling and later histogram binning into one of the allowed pixel ranges given in Table 2. The results after these steps are shown in Figure 2 *c* and *d* respectively.

Figures 3 and 4 summarize the results of the ice-floe size distribution for the regions selected. In Figure 3, histogram of the binned floe sizes is plotted as a function the latitudes of the selected regions. Though the input data for both the plots are same, the left plot is logarithmically scaled to show the distribution of larger sized floes. It can be seen that (1) the low and mid range sized ice floes (below 80 m size) are less dominant over the larger ones when we go towards the pole; (2) the smallest one increases exponentially ($R$-square of exponential fit is 0.994), and (3) there is also slow but steady rise in the number of the mid range floes sized (415 m) towards the polar region. The respective cumulative histogram as a function of floe size for each region selected is shown in Figure 4. It can be seen that the overall number of ice floes increases as the latitude decreases towards the pole to about 85%. The increase in the number of ice floes is sharp from 24 m to 80 m, and then steadies to other large sized floes, similar to lower latitude regions.

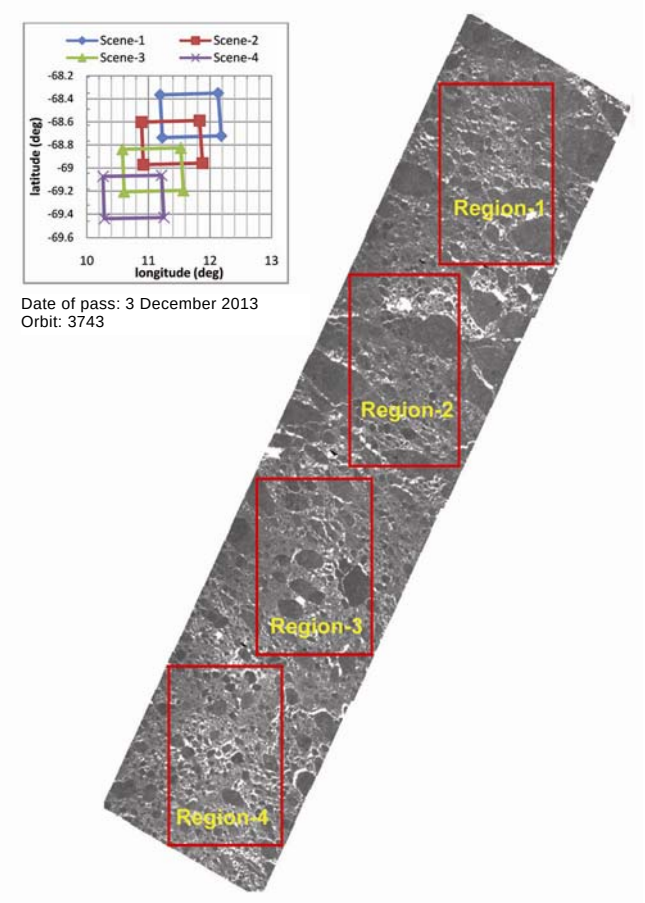


**Figure 1.** RISAT-1 acquired scenes layout with latitude, longitude coordinates (top left) and processed mosaicked image.

**Table 1.** Details about area, dimensions and geographic location of regions shown in Figure 1

| Study area | Dimensions (km) | | Area (sq. km) | Location (°) | |
|---|---|---|---|---|---|
| | Scan | Pixel | | Latitude | Longitude |
| Region-1 | 17.31 | 24.10 | 417.13 | –68.54 | 11.70 |
| Region-2 | 17.24 | 24.34 | 419.65 | –68.79 | 11.37 |
| Region-3 | 17.60 | 24.31 | 427.94 | –69.02 | 11.09 |
| Region-4 | 17.73 | 24.36 | 431.96 | –69.27 | 10.69 |

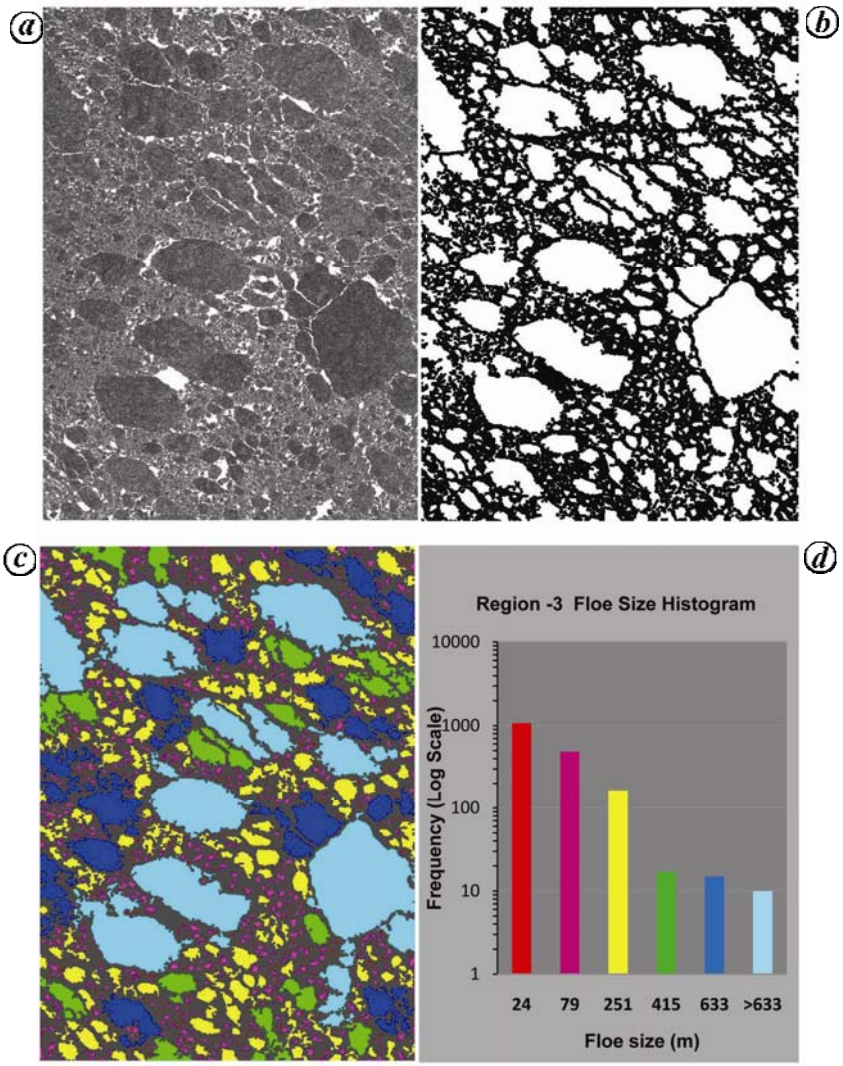


**Figure 2.** ***a***, Original image; ***b***, Local dynamic threshold image; ***c***, Size distribution; ***d***, Histogram of floe size distribution.

To ascertain the accuracy of the automated ice-floe algorithm, in the absence of any field survey data available for this area at the time of acquisition, we have taken up a small area of (500 lines × 500 pixels) from the region, and manually labelled the ice floes with the help of Arc GIS software tools. The overall percentage accuracy of the ice-floe detection was about 80. The small ice floes and very large floes were identified to nearly 90% and above, while the mid range sizes could not be discriminated accurately. The poor discrimination for this category of ice floes may be due to the fact that they touch other floes at many locations and branch out into fragments[5]. However, there is scope for further improvement to overcome these problems. Further research is in progress in this direction.

In summary, the potential of RISAT-1 SAR imagery for identification of sea ice floes and their size distribution has been explored. Instead of manual contouring of ice floes, an automated approach was preferred for operational applications. Initial results with high spatial

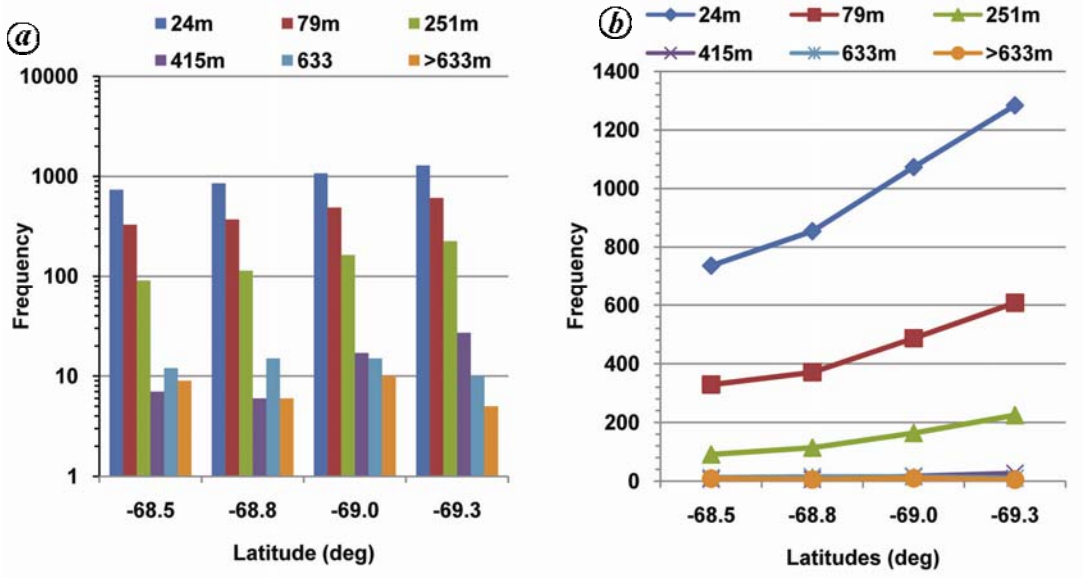


**Figure 3.** Histogram of ice-floe sizes. (***a***) In log scale (for clarity on low values) and (***b***) in linear scale.

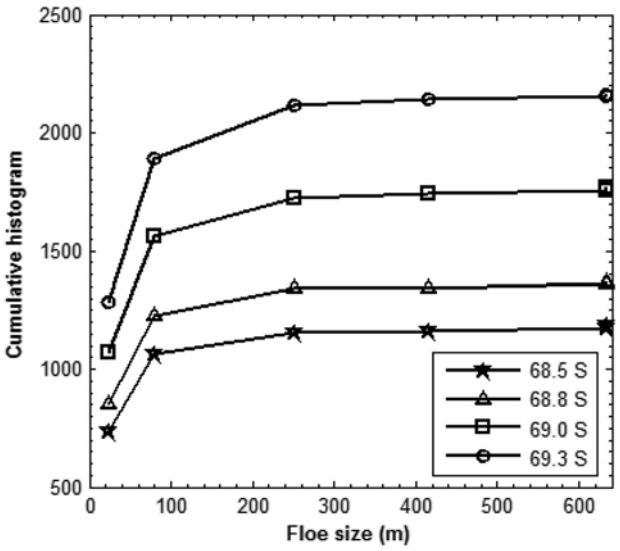


**Figure 4.** Cumulative histogram of floe size distribution with latitude.

**Table 2.** Ice floe size ranges (diameters) for histogram binning

| No. of floe pixels | Median value | Estimated diameter (m) |
|---|---|---|
| < 10 | 5.5 | 24 |
| 11–110 | 60.5 | 79 |
| 111–1110 | 610.6 | 251 |
| 1111–2220 | 1665.6 | 415 |
| 2220–5550 | 3886.1 | 633 |
| >5550 | | >633 |

resolution data have provided some interesting elements in terms of the floe size distribution and its patterns at different latitudes, which will aid in understanding the dynamic processes of sea-ice. Periodic acquisitions are now being planned to study the temporal variations of the ice-floe size distribution and concentration to support ice-floe formation processes and climatic impact studies.

1. Soh, L. K., Tsatsoulis, C. and Holt, B., Identifying ice floes and computing ice floe distributions in SAR images. In *Analysis of SAR Data of the Polar Oceans* (eds Tsatsoulis, C. and Kwok, R.), Springer Verlag, New York, 1998, pp. 9–34.
2. Steel, M., Morison, J. H. and Untersteiner, N., The partition of air ice ocean momentum exchange as a function of ice concentration, floe sizes, and draft. *J. Geophys. Res.*, 1989, **94**, 12739–12750.
3. Toyota, T. and Enomoto, H., Analysis of sea ice floes in the sea of Okhotsk using ADEOS/AVNIR images. In *Ice in the Environment*, Proceedings of the 16th IAHR International Symposium on Ice, Dunedin, New Zealand, 2002.
4. Steel, M., Sea ice melting and floe geometry in a simple ice-ocean model. *J. Geophys. Res.*, 1992, **97**(11), 17729–17738.
5. Brigham, C., Kolkowitz, I, Dolson, M., Rudy, J., Brooks, A., Schmidt, C. and Skiles, J. W., Object-oriented analysis of sea-ice fragmentation using SAR imagery to determine Pacific walrus habitat. In ASPRS Annual Conference, Tampa, Florida, 2007; www.asprs.org/a/publications/proceedings/tampa2007/0009.pdf
6. Misra, T. *et al.*, Synthetic aperture radar payload onboard RISAT-1: configuration, technology and performance. *Curr. Sci.*, 2013, **104**, 446–461.
7. Mahadevan, V., Prasad, T. V. S. R. K., Jain, D. S., Chowdhury, S., Pitchimani, M. and Desai, N. M., Ground segment for RISAT-1 SAR mission. *Curr. Sci.*, 2013, **104**, 477–489.
8. NRSC, Data products and services: RISAT-1, 2013; www.nrsc.gov.in

Received 29 August 2013; accepted 20 September 2013